

# Numerical Prediction of Thermal Storage Using Phase Change Material

S. Sami\* and F. Tardy

Center for Renewable Energy, Catholic University of Cuenca, Cuenca, Ecuador

**Abstract:** A numerical mathematical model has been developed to predict the thermal behavior of phase change material during thermal storage. The model includes the effects of various mechanisms of heat transfer such as conduction, convection as well as fusion of the phase change material. Water/ice was used as a phase change material. The thermal behavior of the phase change material during cooling has been studied experimentally and analyzed under different conditions. Comparisons were made against experimental data for validation of the predictive model. The model fairly predicted experimental data obtained at various inlet conditions.

**Keywords:** Phase change material, thermal storage, numerical model, simulation.

## 1. INTRODUCTION

The increasing demand for energy efficiency and renewable energies is the main drive for continuously introducing and developing new renewable energy technologies. Thermal and energy storage are not only play an important role in the renewable energy field but also improve performance, enhance reliability heat recovery systems [1-5] and become significant in solar energy applications and electrification of remote areas [6,7].

Heat pipe heat exchangers are efficient energy techniques used in heat recovery system. The advantage of using heat pipes over conventional methods is that large quantity of heat that can be transported through a small cross-sectional area over a considerable distance without moving parts and the need for additional power into the system [7-14].

Numerous studies have presented on the use of heat pipe heat exchangers for heat recovery. Yang *et al.* [13] used heat pipe heat exchanger for recovery of waste heat in heating automobile using exhaust flue gas. Furthermore, heat pipe heat exchangers were also used by Mostafa *et al.* [14] for heat recovery in air conditioning applications. Finally, Liu *et al.* [15] studied the application of heat pipe heat exchanger for flue gas heat recovery system and presented thermodynamic analysis of the process. The main objective of this paper is to study of the performance of heat pipe heat exchanger and phase change material in the cooling process of air conditioning trucks to reduce fuel consumption. Trucks are used for transport goods for

long haul and generally equipped with berths so that the truck-driver can sleep during travel. In hot summer days, the high temperature and humidity requires truck-drivers to idle their engines for long periods for air-conditioning purposes. Excessive idling, however, consumes significant amounts of fuel and negatively impacts the environmental due to emission of greenhouse gases. We propose a system using storage tank with phase change material that can store heat during daily operation and recover later to meet cooling load requirements. During daily operation heat is transferred to the storage tank to melt the ice-water in the storage tank. During the night, heat is recovered from the storage tank and phase change material to provide air conditioning without idling the engine.

A mathematical model for predicting the heat recovery from the storage tank is presented hereby. In addition, an experimental set up was constructed in order to validate the mathematical model. The mathematical model was used to study of the effect of operating conditions on the phase change material and system performance.

## 2. MATHEMATICAL MODEL

A schematic of the system under study is depicted in Figure 1. The system consists of an insulated ice storage tank where the condenser section of heat pipes heat exchanger is placed. The evaporator section of the heat pipes heat exchanger is mounted in an insulated air duct. The moist air, referred as coolant, enters the duct at mass flow rate  $\dot{m}$ , temperature  $T_{in}$  and relative humidity  $\phi_{in}$  passes through the heat exchanger where it release its heat and leaves at conditions  $T_{out}$  and  $\phi_{out}$ .

To determine the psychrometric properties of the moist air, the following is presented. The humidity of

\*Address correspondence to this author at the Center for Renewable Energy, Catholic University of Cuenca, Cuenca, Ecuador; Tel: 760 476 9256; Fax: 760 476 9257; E-mail: dr.ssami@transpacenergy.com, dr.samuelsami@icloud.com

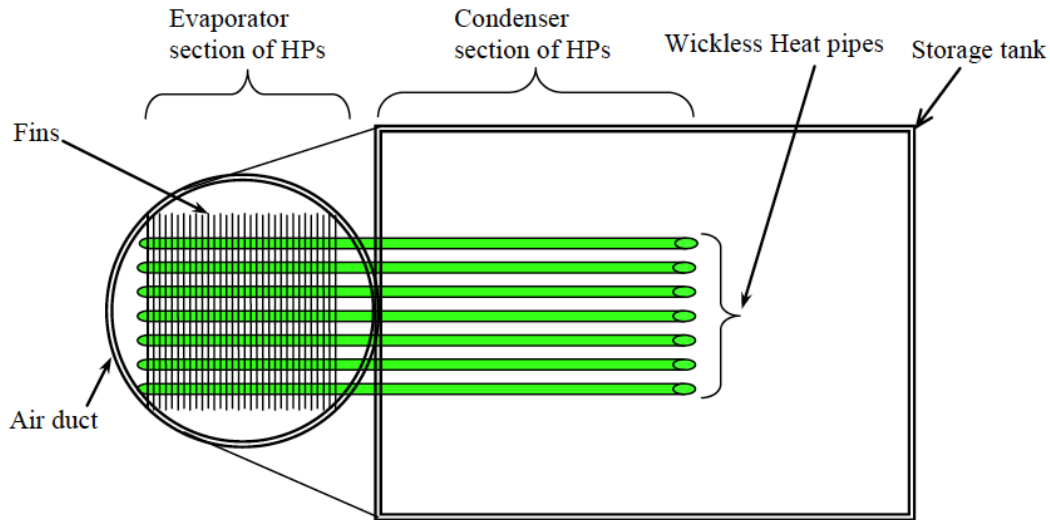


Figure 1: schematic of experimental set up system.

the air is determined by the dew point temperature,  $T_{dew}$ , when the air mean surface temperature,  $T_1$ , is less than  $T_{dew}$ , condensation of the water vapour occurs, and thus dehumidification, is attained and referred to as dehumidification cooling. Otherwise, if  $T_1$  is greater than  $T_{dew}$ , no condensation occur and the cooling is carried out by sensible heat.

In the sensible cooling, dew temperature can be evaluated by:

$$T_d = C_1 + C_2\alpha + C_3\alpha^2 + C_4\alpha^3 + C_5p_w^{0.1984} \quad (1)$$

for the dew-point temperature range between 0 to 93 °C.

where;

$$\alpha = \ln(p_w), \quad C_1 = 6.54, \quad C_2 = 14.526, \quad C_3 = 0.7389, \\ C_4 = 0.09486, \quad C_5 = 0.4569 \text{ and}$$

$$p_w = \frac{pw}{0.6298 + w}$$

### a) Sensible Cooling

The steady state energy and mass balance of coolant between the inlet and the outlet the cooling coil can be written as:

$$\dot{m}_a c_{pa} (T_{in} - T_{out}) = \dot{q} \quad (2a)$$

$$\text{or} \quad T_{out} = T_{in} - \frac{\dot{q}}{\dot{m}_a c_{pa}} \quad (2b)$$

and

$$w_{in} = w_{out} = w \quad (2c)$$

where;  $\dot{q}$  is the rate of energy transferred to the storage tank with phase change material

at given  $\phi_{in}$ , one can evaluate  $w_{in}$  by the relationship between  $\phi$  and  $w$  as:

$$w = 0.62198 \frac{\phi p_{ws}}{p - \phi p_{ws}} \quad (3)$$

Where;  $p_{ws}$  is the saturated water pressure. For temperature range of 0 to 200C is given by;

$$\ln(p_{ws}) = C_1 / T + C_2 + C_3 T + C_4 T^2 + C_5 T^3 + C_6 \ln T \quad (4)$$

Where;

$T$  is in the absolute temperature, K and

$$C_1 = 5.800220610^3, \quad C_2 = 1.3914993, \quad C_3 = -4.864023910^{-2}, \\ C_4 = 4.176476810^{-5} \quad C_5 = -1.445209310^{-8} \text{ and} \\ C_6 = 6.5459673$$

Using Equations (1b) and (2), one can evaluate  $T_{out}$  and  $w_{out}$  and the psychrometric properties of the moist air at the outlet of the cooling coil.

### b) Dehumidification Cooling

The process of dehumidification cooling is described in the Figure 2. The moist air can reach the point c if the coil has an infinite surface. This point is used only to evaluate the slope of the curve (ab):

$$\frac{\Delta w}{\Delta T} = \frac{w_1 - w_{in}}{T_1 - T_{in}} \quad (5)$$

Where  $w_1$  is the humidity ratio evaluated at  $T_1$  for  $\phi = 100\%$ .

With reference to Figure 1,  $\frac{\partial w}{\partial T}$  can be written as:

$$\frac{\Delta w}{\Delta T} = \frac{w_{out} - w_{in}}{T_{out} - T_{in}} \quad (6a)$$

or

$$w_{out} = (T_{out} - T_{in}) \frac{\Delta w}{\Delta T} + w_{in} \quad (6b)$$

The enthalpy for the moist air is expressed as:

$$h = h_a + wh_g \quad (7a)$$

Where,  $h_a$  is the specific enthalpy of dry air and  $h_g$  is the specific enthalpy of saturated water vapour at the temperature of the mixture.

$$h_a = c_{pa}T \quad (7b)$$

$$h_g = 2501 + 1.805T \quad (7c)$$

The enthalpy for the moist air at the inlet and the outlet of the cooling coil can be written as:

$$h_{in} = c_{pa}T_{in} + w_{in}(2501 + 1.805T_{in}) \quad (8a)$$

$$h_{out} = c_{pa}T_{out} + w_{out}(2501 + 1.805T_{out}) \quad (8b)$$

where

$$h_{out} = h_{in} - \frac{\dot{q}}{\dot{m}} \quad (9)$$

Knowing  $\dot{q}$ , the outlet psychometric properties ( $T_{out}$  and  $w_{out}$ ) can be obtained by combining Equations (6b) and (8b).

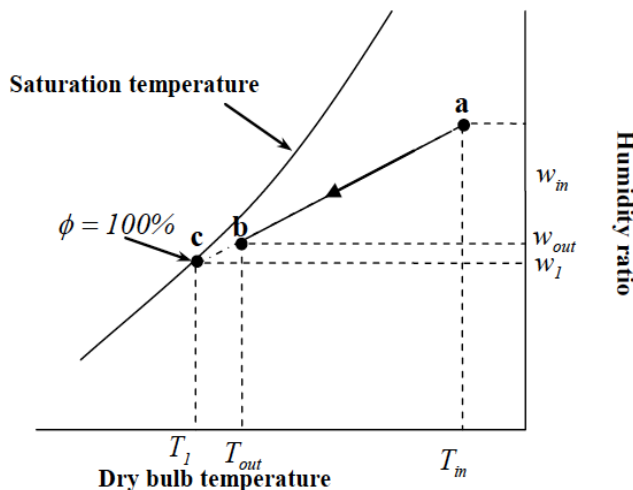


Figure 2: cooling with dehumidification.

### 2.1. Calculation of $\dot{q}$

During the heat transfer process, the heat is transferred from the hot air to the heat pipes heat exchanger placed in the ice tank and can be evaluated by;

$$\dot{q} = \frac{T_{air.in} - T_{ref}}{R(t)} = \dot{q}_s + \dot{q}_l \quad (10)$$

Where;  $\dot{q}_s$  and  $\dot{q}_l$  are instantaneously sensible and latent heat absorbed, respectively.

As shown in Figure 2a, the overall heat resistance  $R(t)$  consists of three parts: the heat resistance of the heat exchanger, the heat resistance of heat pipes and heat resistance of water (phase change material) formed into the ice tank.

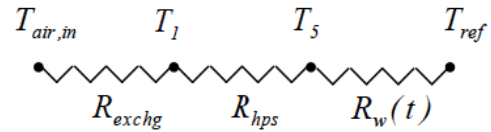


Figure 2a: schematic of thermal resistances between  $T_{air.in}$  and  $T_{ref}$ .

Where  $T_1$  and  $T_5$  are the outside surface temperatures of the evaporator and condenser heat pipes sections respectively.  $T_{ref}$  and  $T_{air.in}$  represent the phase change material and the air inlet temperatures and  $R(t)$  is the thermal resistance between air inlet of channel and the phase change material in the tank and can be expressed as follows:

$$R(t) = R_{exchg} + R_{hps} + R_w(t) \quad (11)$$

Where;  $R_{exchg}$ ,  $R_{hp}$  and  $R_w(t)$  are the thermal resistance due to of the heat exchanger heat pipes and the mass of water in the tank, respectively. The latter depends on ice melted in the tank and time. It can also be noted that the Equation (10) is not valid if all ice in the tank is fully melted. In this case one can write energy balance as:

$$\rho C_p \frac{\partial \bar{T}_w}{\partial t} = \frac{T_{air.in} - \bar{T}_w}{R(t)} = \dot{q} \quad (12)$$

Where,  $\bar{T}_w$  is the mean temperature between  $T_{ref}$  and  $T_5$

In addition, the amount of energy required to melt a mass  $m(t)$  of ice (latent heat) and increase its temperature from  $T_{ref}$  to  $\bar{T}_w$  (sensible heat) can be given by:

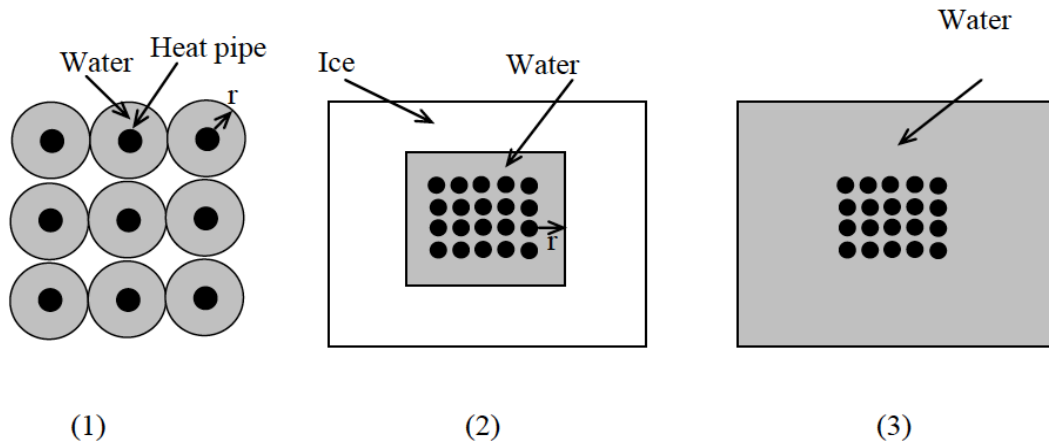


Figure 3: Process of melting of ice in the tank.

$$Q = m(t)h_{sl} + m(t)C_{pw}(\bar{T}_w - T_{ref}) \quad (13)$$

This energy corresponds to the integration of heat transfer rate  $\dot{q}$  between 0 and time  $t$ :

$$\int_0^t \dot{q} dt = Q \quad (13.1)$$

To calculate the time  $t$  required to melt a mass  $m(t)$  of ice and increase its temperature from  $T_{ref}$  to  $\bar{T}_w$ , one can rewrite Equation (4) as;

$$\delta Q = \dot{q} \delta t \quad (13.2)$$

or

$$\frac{\delta Q}{\dot{q}} = \delta t \quad (13.3)$$

For numerical considerations, Equation (13.3) can be written as:

$$t - t^0 = \frac{Q - Q^0}{(\dot{q} + \dot{q}^0)/2} \quad (14)$$

or

$$t = \frac{Q - Q^0}{(\dot{q} + \dot{q}^0)/2} + t^0 \quad (15)$$

Where,  $Q^0$  and  $\dot{q}^0$  are the total energy the rate of heat transfer to the tank calculated in the preceding time  $t^0$ .

### 2.1. Resistances Calculation

The discharging process of the tank can be divided into three stages: (1) formation of quasi-concentric

layers water layer around heat pipes. This stage is reached when the water layers reach the heat pipes; (2) considers that all ice between and around the water layer is melted, the process of melting is considered as cubic prism. This cubic prism grow with melting of ice until no ice exist in the tank; (3) during this stage the heat transfer occurred between heat pipes and cold water as sensible heat. This stage is reached when the temperature of water becomes equal to the temperature of the inlet air  $T_{air.in}$  (C.F, Figure 3).

#### 2.1.1. Water Resistance in the Storage Tank

**Stage 1:** for  $r \leq r_1$  assumes that the ice melting around the heat pipes is *quasi-concentric cylinder* as shown in Figures 3 and 4. The thermal resistance of the water is, therefore, can be written as:

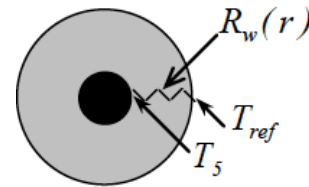


Figure 4: schematic of ice melting around heat pipe.

$$R_w(r) = \frac{\ln\left(\frac{r_{hp,ex} + r}{r_{hp,ex}}\right)}{2\pi k_{w,eff} L_c N} \quad (16)$$

Where,  $k_{w1,eff}$  takes into account natural convection in the water layer. It is the effective thermal conductivity that a stationary fluid should have to transfer heat as a moving fluid. The suggested correlation for  $k_{w1,eff}$  is obtained after Incroperat and DeWitt [8]:

$$k_{w1,eff} = 0.386 k_w \left(\frac{Pr}{0.861 + Pr}\right)^{1/4} (Ra_c^*)^{1/4} \quad (17)$$

where

$$Ra_c^* = \frac{\left[ \ln \left( \frac{d_{hp,ex} + 2r}{d_{hp,ex}} \right) \right]^4}{(rN)^3 \left[ (d_{hp,ex} + 2r)^{-3/5} + (d_{hp,ex})^{-3/5} \right]^5} Ra_r \quad (18)$$

$$Ra_r = \frac{r^3 \rho_w \beta_w g C_{pw} (T_5 - T_{ref})}{\mu_w k_w} \quad (19)$$

Equation (17) may be used for the range  $10^2 \leq Ra_c^* \leq 10^7$ . For  $Ra_c^* < 10^2$ ,  $k_{w1,eff} = k_w$ .

**Stage 2.**  $r_1 < r < r_4$

During this stage 2, the process of melting is not considered as quasi-concentric cylinder but as cubic prism. In this case the resistance is evaluated by:

$$R_w(r) = \frac{1}{k_{w2,eff} S} + R_w(r_1) \quad (20)$$

Where S is the shape factor given by Holman [2002] for conduction through the edge of adjoining walls (C.F. Figures 4a and b) where  $S_{edge} = 0.54D$

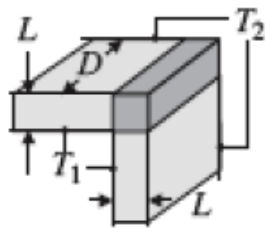


**Figure 4a:** Schematic of Stage -2, conduction through corner of three walls  $S_{corner} = 0.15L$ .

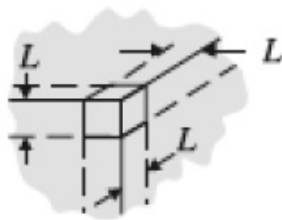


**Figure 4b:** Schematic of conduction through the wall For conduction through the walls.

Where,  $S_{wall} = A / L$

And; A is the surface of the wall.

The shape factor is evaluated as:

$$S_2 = S_{walls,2} + S_{edges,2} + S_{corners,2} \quad (21)$$

Where  $k_{w2,eff}$  is obtained using a correlation given by Holman [12]:

$$k_{w2,eff} = 0.046 * k * Ra_2^{(1/3)} \quad (22)$$

Where

$$Ra_r = \frac{L_{eff}^3 \rho_w \beta_w g C_{pw} (T_5 - T_{ref})}{\mu_w k_w} \quad (23)$$

$L_{eff}$  is an effective length and depends on conditions described in the following cases:

**Case 1:** For  $r_1 < r \leq r_2$  where we have 5 walls, 8 edges and 4 corners

In this case  $L_{eff}$  is expressed as:

$$L_{eff} = \frac{1}{\frac{1}{2(L_{cHP} + 2(r - r_1)) + (La_{HP} + 2(r - r_1))} + \frac{1}{H_{HP} + 2(r - r_1)}} \quad (24)$$

**Case 2:** for  $r_2 < r \leq r_3$  the top and the bottom wall is molten where we have 3 walls, 8 edges and 4 corners. In this case  $L_{eff}$  is expressed as:

$$L_{eff} = \frac{1}{\frac{1}{2(L_{cHP} + 2(r - r_1)) + (La_{HP} + 2(r - r_1))} + \frac{1}{H_{tank}}} \quad (25)$$

**Case 3:** for  $r_3 < r \leq r_4$  it remains only one wall and we have 1 wall, 4 edges and 4 corners

In this case  $L_{eff}$  is expressed as:

$$L_{eff} = \frac{1}{\frac{1}{La_{tank}} + \frac{1}{H_{tank}}} \quad (26)$$

**Stage 3:** In this phase, the ice in the tank is entirely melted. The heat transfer is regarded as natural convection between the water in the tank and a group of layers around cylindrical heat pipes. In this case,

$$R_w = \frac{1}{h_w d_{hp,ext} \pi L_{cHP} N} \quad (27)$$

where

$$h_w = F \frac{Nu_w k_w}{d_{hp,ext}} \quad (28)$$

F is the correction factor used to ensure a continuity in the heat flux in the phase 3. And can be expressed as:

$$F = \frac{R_{w3s} \dot{q}_{4f}}{T_{air,in} - \bar{T}_{w,4f}} \quad (29)$$

Where;  $R_{w3s}$ ,  $\dot{q}_{4f}$ ,  $\bar{T}_{w,4f}$

and

$$Nu_w = 0.53 Ra_{dhp}^{1/4} \quad (30)$$

$Ra_{dhp}$  is the Rayleigh number base on heat pipes diameter.

### 2.1.2. Heat Pipes Resistance

The overall thermal resistance of thermosyphone occurring in the heat pipe is comprised typically of resistances arranged in a series combination and can be summarized as:

$$R_{hp} = R_{we} + R_{ie} + R_{va} + R_{ic} + R_{wc} \quad (31)$$

Where;

$R_{we}$  : heat pipe wall radial resistance, evaporator;

$R_{ie}$  : liquid-vapor interface resistance, evaporator;

$R_{va}$  : adiabatic vapor section resistance;

$R_{ic}$  : liquid-vapor interface resistance, condenser;

$R_{wc}$  : heat pipe wall radial resistance, condenser;

According to Peterson [11], the order of magnitude of liquid-vapor interface resistance ( $10^{-5}$ ) and adiabatic vapor section resistance ( $10^{-8}$ ) is so small compared to heat pipe wall radial resistance. Therefore, the primary resistances of heat pipe are heat pipe wall radial resistances are;

$$R_{hp} = R_{we} + R_{wc} \quad (32)$$

where

$$R_w = \frac{\ln(r_{hp,out} / r_{hp,in})}{2\pi kL} \quad (33)$$

Since we have  $N$  number of heat pipe,  $R_w$  becomes:

$$R_w = \frac{\ln(r_{hp,out} / r_{hp,in})}{2\pi kLN} \quad (34)$$

### 2.1.3. Heat Exchanger Resistance

Because of fins associated with the evaporator section of the heat pipe heat exchanger, the thermal resistance can be written as:

$$R_{exch} = \frac{1}{\eta_o h_{air} A_{fins}} \quad (35)$$

$$\eta_o = 1 - \frac{A_f}{A} (1 - \eta_f) \quad (36)$$

where  $\eta_f$  is fins efficiency approximated by McQuiston and Tree [10]:

$$\eta_f = \frac{\tan(m\psi_f)}{m\psi_f} \quad (37)$$

$$\psi_f = r_{hp,out} \left( \frac{1 - \rho}{\rho} \right) \left( 1 + 0.35 \ln \frac{1}{\rho} \right) \quad (38)$$

$$\rho = \frac{r_{hp,out}}{\left( \frac{S_T}{2} \sqrt{\frac{2\sqrt{3}}{\pi}} \right)} \quad (39)$$

$$m = \left( \frac{2h_{air}}{k_f e_f} \right) \quad (40)$$

However,  $h_{air}$  is calculated as:

$$h_{air} = j \frac{c_{Pair} G}{Pr_{air}^{2/3}} \quad (41)$$

And,  $j$  is a Colburn factor given as per Kreith [11]:

$$j = 0.14 Re_d^{-0.328} \left( \frac{S_T}{S_L} \right)^{-0.502} \left( \frac{s}{d_{hp,out}} \right) \quad (42)$$

where  $s$  is the distance between adjacent fins.

$Re_d$  is the Reynolds number given by:

$$Re_d = \frac{\dot{m} d_{hp,out}}{\mu_{air} A_e} \quad (43)$$

Where  $A_e$  is the cross sectional area perpendicular to the flow direction and  $\dot{m}$  is the mass flow rate.

## 3. NUMERICAL PROCEDURE

The numerical procedure to calculate  $\dot{q}$  is as follow; first initialize the temperature filed and for a given  $r$  one can calculate the value of the resistance  $R_w$  according to the interval where  $r$  is situated. Then calculate  $R_{exchg}$  and  $R_{hps}$ . This follows by calculating  $\dot{q}$  and  $Q$  and calculate the time  $t$  corresponding to the distance  $r$ . This procedure continues until there is no

more ice in the tank and calculates  $\dot{q}$  using Equation (12). Once  $\dot{q}$  is given and for given  $T_{air,in}$  and  $\phi_{in}$ , the psychrometric properties of the air at the outlet are determined using the Equation (4) if sensible cooling is occurred or Equation (9) if dehumidification cooling is occurred.

#### 4. EXPERIMENTAL ST-UP

An experimental rig is set up to further check the validity of the numerical model as shown in Figures 1 and 4c. It consists of an ice storage tank 0.3 m high, 0.6 dept and 0.6 wide connected to the condenser section of heat exchanger compose of 36 wickless heat pipes 0.8 cm diameter and 0.6m length. The evaporator section of the heat pipe heat exchanger is connected to an air duct 3.66 m length and 0.15 m diameter. Two fans are mounted in series in order to circulate the air between inlet and outlet of the duct. To minimize the heat loss by radiation and convection to surrounding air, the storage tank has been insulated with styro foam of 2.54 cm thickness and the air duct with glass wool of 1 cm thickness. The heat pipes were charged with a binary refrigerant mixture; R23/R152a that has the same thermo physical properties like R-22. The heat pipe heat exchanger is tilted by an angle of 7 in order to have an optimal heat transfer inside heat pipes. Temperature in the tank are measured by means of 10 thermocouple (type K) located in different position. 4 thermocouples (type K), 2 with dry bulb and 2 with wet bulb, are used to measure the temperature and humidity ratio at the inlet and outlet of the air duct. All thermocouples are connected to a data acquisition system. Thermocouples are accurate within  $\pm 0.5$  C. To study the ice-water interface various thermocouples type T were placed in the water reservoir where the heat pipe condenser was immersed. The accuracy of the thermocouples was of  $\pm 0.5\%$  full scale. The accuracy of air mass flow measurement was  $\pm 3\%$  of the nominal flow. The uncertainty analysis conducted for the experimental data used in this study revealed an accuracy of  $\pm 4\%$  of full scale.

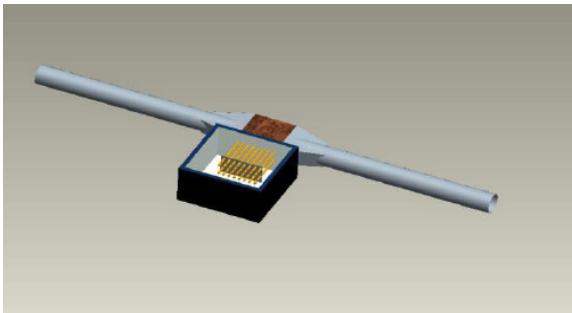


Figure 4c: Schematic of experimental set up.

Data collection was carried out using the Lab View acquisition system. This enabled us to record with a single scan, local properties. All tests were performed under steady state conditions. The channels were scanned every second and stored every 10 seconds. Tests started with ice in the reservoir at  $-1^{\circ}\text{C}$ . All recorded measurements were obtained according to the ARI and ASHRAE Standards.

#### 5. DISCUSSION AND ANALYSIS

The aforementioned system of equations has been numerically solved and samples of the predicted results are plotted in Figures 5 through 8, and compared with experimental data for a cooling cycle at different inlet conditions. In general, it is quite clear from these figures that initially the experimental data were under predicted for the first 30 minutes. This was attributed to the fact that the heat flux diminishes faster than the rate of heat transfer predicted by the model especially as the ice reaches the tank walls. Furthermore, the data presented in these figures also showed that after 30 minutes the data continued to be under predicted and stabilized after 1.2 hours. However, after two hours the heat transfer rate stabilized at 0,38 kW for up to 10 hours. At this point the heat transfer rate diminished during the next five hours until the cooling cycle ends. The numerical model's prediction showed that the phase change material/ice was fully melted after 12h:48 minutes after the cooling cycle started. Furthermore, the model predicted that the heat transfer with air was reduced to 100 watts at 16h:12 minutes. This was in fair agreement with the experimental data.

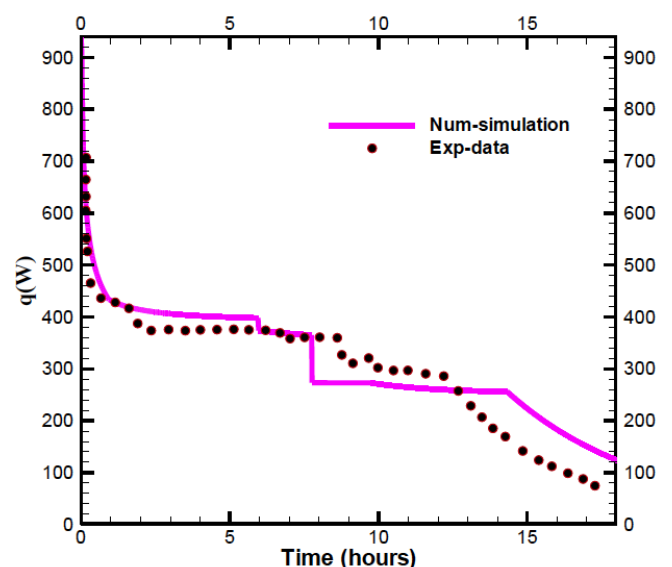
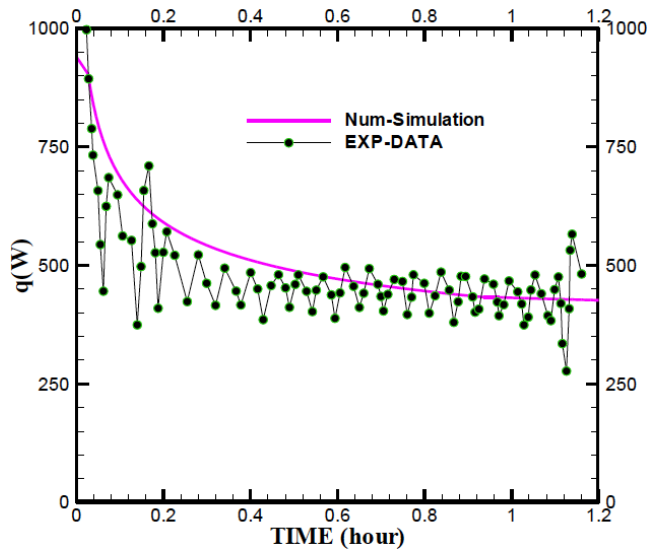
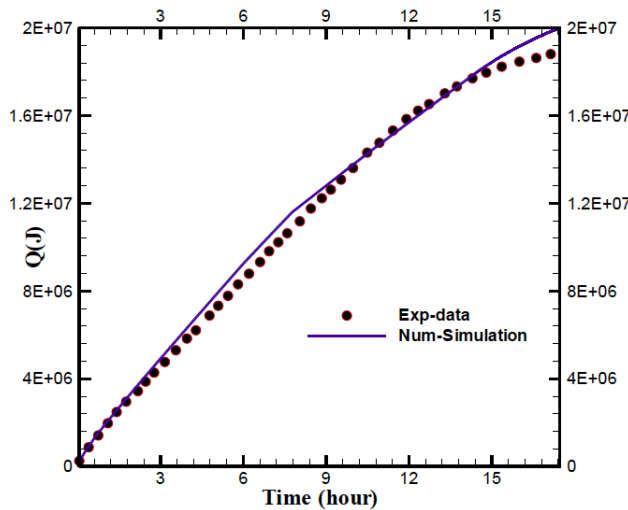


Figure 5: energy rate transferred to the storage tank versus time for  $\phi_{in} = 75\%$ ,  $T_{air,in} \approx 24^{\circ}\text{C}$  and  $\dot{m} = 0.0766\text{Kg}\cdot\text{s}^{-1}$ .



**Figure 6:** energy rate transferred to the storage tank versus time for  $\phi_{in} = 75\%$ ,  $T_{air\_in} \approx 24^{\circ}C$  and  $\dot{m} = 0.0766Kg.s^{-1}$ .



**Figure 7:** Total of energy transferred to the storage tank versus time for  $\phi_{in} = 75\%$ ,  $T_{air\_in} \approx 24^{\circ}C$  and  $\dot{m} = 0.0766Kg.s^{-1}$ .

The heat transfer rate absorbed from the air flow and transferred to phase change material/ice in the reservoir has been plotted as a function of cooling cycle time and compared to the model's prediction in Figure 8. This figure showed that the model fairly predicted outlet relative humidity and temperature. Figure 7 also showed that in general the model prediction of the total energy transferred to the storage tank was satisfactory, during the cooling cycle.

The predicted results and data showed that the heat transfer rates at certain time intervals are equal to the heat flux at the surface. As the heat flux remained relatively constant during the cooling cycle, heat transfer was relatively linear over the cooling cycle

period for the last ten hours of the experience. Since the heat flux was relatively constant during the experiment it can be concluded that heat transfer rates had temporal linear dependence during the cooling cycle.

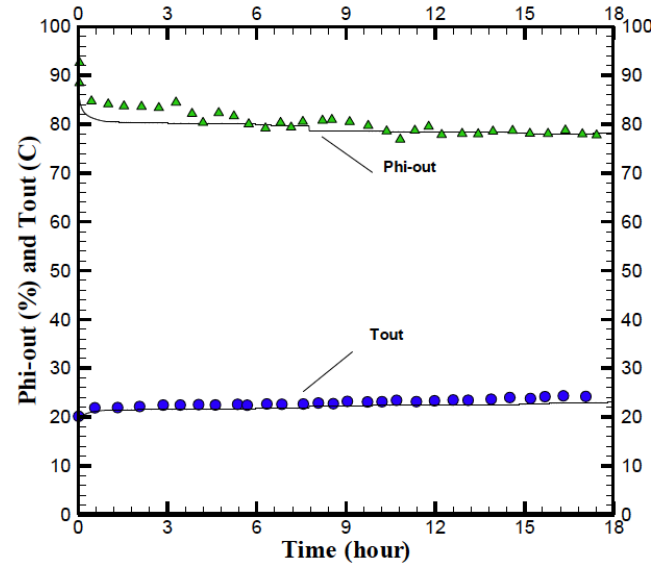


**Figure 8:** Outlet relative humidity and temperature versus time for  $\phi_{in} = 75\%$ ,  $T_{air\_in} \approx 24^{\circ}C$  and  $\dot{m} = 0.0766Kg.s^{-1}$ .

Furthermore, in order to study the impact of air inlet mass flow rate at on the phase change material and heat transferred during the cooling cycle, Figures 9 through 10 were constructed at different air mass flow rates and relative humidity of 30% and 70%. The data displayed in these figures showed that at a particular time frame, higher air mass flow increased the outlet air temperature and the energy transferred to the storage

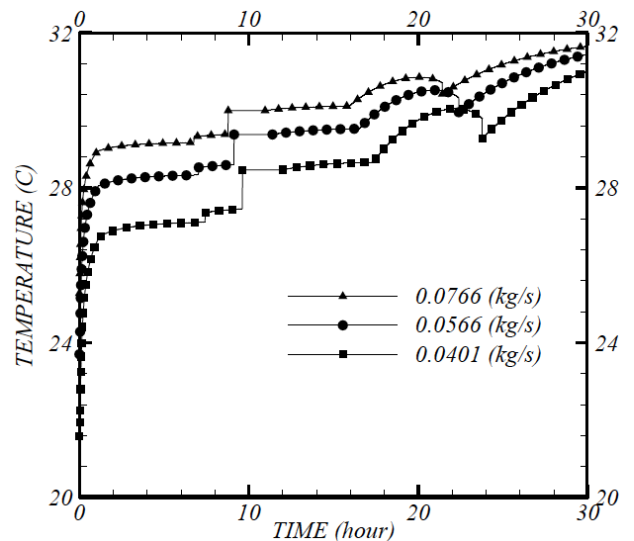


**Figure 9:** Outlet temperature versus time for various mass flow rate and  $T_{in} = 32^{\circ}C$  and  $\phi_{in} = 70\%$ .

material in the tank. Similarly, Figures 11 through 14 were presented to demonstrate the effect of increasing the air mass flow rate on the humidity ratio between the inlet and outlet conditions at different relative humidity entering air flow. The data in these figures showed that depending on the initial relative humidity the cooling cycle time can be impacted.

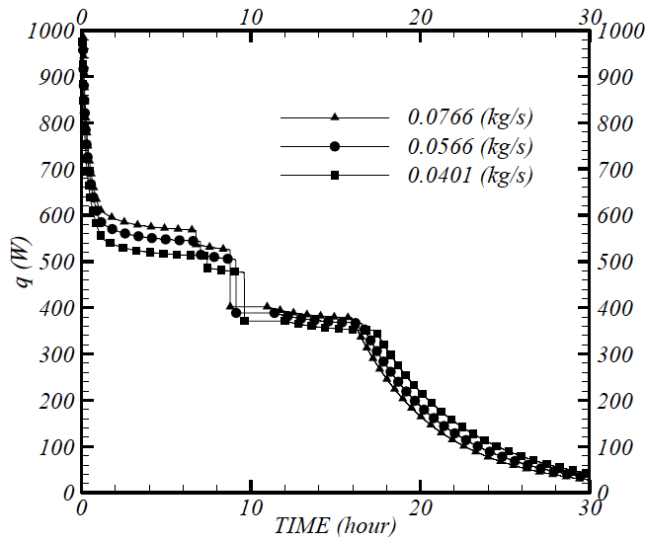


Figure 10: energy rate transferred to the phase change material versus time for various mass flow rate and  $T_{in}=32$  C and  $\phi_{in}=70\%$ .

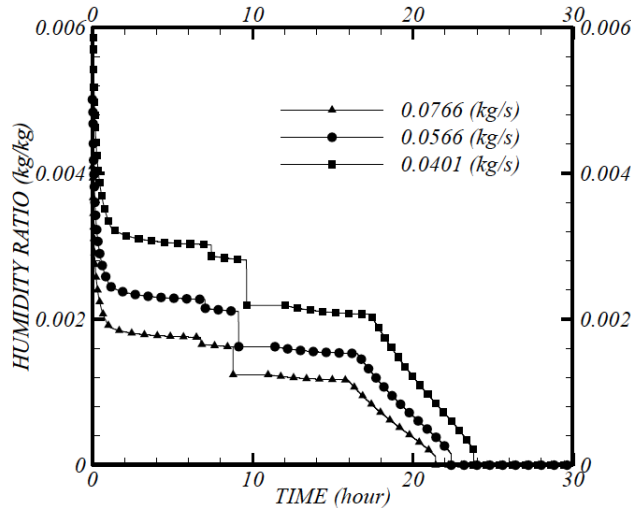


Figure 11:  $(W_{in} - W_{out})$  versus time for various mass flow rate and  $T_{in}=32$  C and  $\phi_{in}=70\%$ .

CONCLUSIONS

During the course of this study, the heat transfer characteristics of heat pipes and phase change material in a thermal storage process have been modeled, presented and analyzed. An experimental setup has been constructed and various tests of thermal storage cooling cycle have been carried out

under different inlet conditions. In general, the presented numerical model fairly predicted the heat transfer characteristics during phase change material and interactions between the ice and heat pipes as well as air flow and compared well with the experimental data.

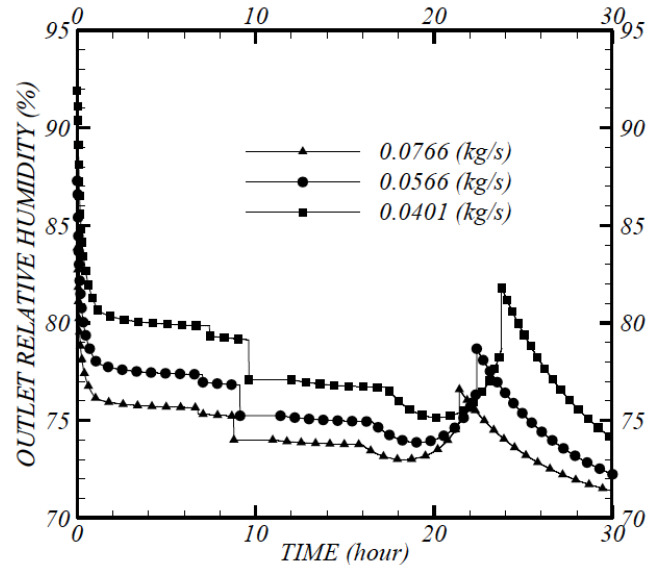


Figure 12: Outlet relative humidity versus time for various mass flow rate and  $T_{in}=32$  C and  $\phi_{in}=70\%$ .

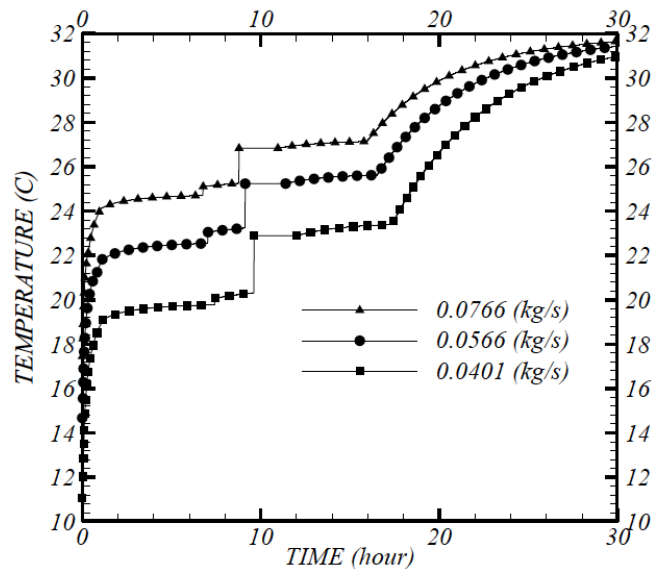
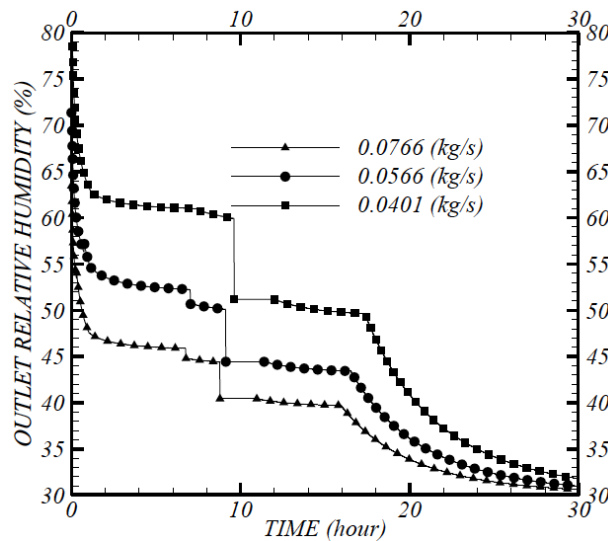


Figure 13: Outlet temperature versus time for various mass flow rate and  $T_{in}=32$  C and  $\phi_{in}=30\%$ .

The predicted results and data showed that the heat transfer rates at certain time intervals are equal to the heat flux at the surface. As the heat flux remained relatively constant during the cooling cycle, heat transfer was relatively linear over the cooling cycle period for significant period of the experience.



**Figure 14:** Outlet relative humidity versus time for various mass flow rate and  $T_{in}=32\text{ C}$  and  $\phi_{in}=30\%$ .

## NOMENCLATURE

$A$	= Heat transfer area ( $\text{m}^2$ )
$A_{fins}$	= Fin heat transfer area ( $\text{m}^2$ )
$C_{pair}$	= Specific heat of air ( $\text{J/kg}\cdot\text{C}$ )
$D$	= Diameter of heat pipes (m)
$G$	= Mass flux ( $\text{kg m}^{-2}\text{ s}^{-1}$ )
$h$	= Heat transfer coefficient ( $\text{kW m}^{-2}\text{ K}^{-1}$ )
$H$	= Total air enthalpy ( $\text{kJ kg}^{-1}$ )
$k$	= Thermal conductivity of liquid ( $\text{kW m}^{-1}\text{ K}^{-1}$ )
$L_c$	= Condenser length (m)
$L_e$	= Evaporator length (m)
$L$	= Length (m)
$\dot{m}_{air}$	= Mass flow rate ( $\text{kg s}^{-1}$ )
$M$	= Viscosity ( $\text{kg/m s}$ )
$N$	= Number of heat pipes
$\dot{q}_r$	= Total heat transfer (W)
$S$	= Outside surface area around the heat pipes ( $\text{m}^2$ )
$R_{cond}$	= Wall thermal resistance ( $\text{K kW}^{-1}$ )
$R$	= Thermal resistance ( $\text{K kW}^{-1}$ )

$T_{fins}$  = Temperature ( $^{\circ}\text{C}$  or  $\text{K}$ )

$x$  = Distance between heat pipes and ice wall (m)

## Subscripts

air = Air

fins = Fins

cond = Condenser

cond,int = Condenser internal area

evap = Evaporator

evap,int = evaporator internal area

oper = operating temperature

tube-evap = Evaporator tube wall

tube-cond = Condenser tube wall

ice = Ice

g = Melt ice/water

HP = Heat pipe

HP,int = Heat pipe internal surface

HP,ext = Heat pipe external surface

w = Water

## ACKNOWLEDGEMENT

The research work presented in this paper was made possible in part through the support of the Catholic University of Cuenca.

## REFERENCES

- [1] Farid MM, Khudhair AM, Razack SA, Al-Hallaj S. A review on phase change energy storage material. *Energy Conversion and Management* 2004; 45: 1597. <http://dx.doi.org/10.1016/j.enconman.2003.09.015>
- [2] Sauciu I, Akbarzadeh A, Johnson P. Characteristics of two-phase closed hermosyphons for medium temperature heat recovery applications. *Heat Recovery Systems and CHP* 1995; 15(7): 631-640. [http://dx.doi.org/10.1016/0890-4332\(95\)90043-8](http://dx.doi.org/10.1016/0890-4332(95)90043-8)
- [3] Bellecci C, Conti M. Transient behaviour analysis of a latent heat thermal storage module. *International Journal of Heat Mass Transfer* 1993; (36): 3851-3857. [http://dx.doi.org/10.1016/0017-9310\(93\)90065-E](http://dx.doi.org/10.1016/0017-9310(93)90065-E)
- [4] Elawadhi EM. Phase change process with free convection in a circular enclosure; numerical simulation. *Computer & Fluids* 2005; (33): 1335-148.

- [5] Tardy F, Sami SM. An experimental study determining behaviour of heat pipes in thermal storage. *International Journal of Ambient Energy* 2008; 29(3).  
<http://dx.doi.org/10.1080/01430750.2008.9675072>
- [6] Razali T, Hamdani, Irwasnsyah, Zaini. Investigation of performance of solar water heater system using paraffin wax. *ARPN Journal of Engineering and Applied Sciences* 2014; 9(10).
- [7] Thirugnanm C, Marimuthu P. Experimental analysis of latent heat thermal energy storage using paraffin wax as phase change material. *International Journal of Engineering and Innovative Technology (IJEIT)* 2013; 3(2).
- [8] Incropera PF, DeWitt DP. *Fundamentals of heat and mass transfer*, Fourth edition, John Wiley & Sons, Inc. New York 1999.
- [9] Kreith F. *Mechanical engineering handbook*, Heat and mass transfer, CRC Press LLC 1999.
- [10] McQuiston FC, Tree DR. Optimum Space Envelopes of the Finned Tube Heat Transfer Surface. *Trans ASHRAE* 1972; 78: 144-148.
- [11] Peterson GP. *An Introduction to Heat Pipe*, Wiley, New York 1994.
- [12] Holman JP. *Heat Transfer*, Ninth Edition, McGraw-Hill, New York 2002.
- [13] Yang F, Yuan X, Lin G. Waste heat recovery using heat pipe heat exchanger for heating automobile using exhaust gas. *Applied Thermal Engineering* 2003; 23: 367-372.  
[http://dx.doi.org/10.1016/S1359-4311\(02\)00190-4](http://dx.doi.org/10.1016/S1359-4311(02)00190-4)
- [14] Abd El-Baky MA, Mohamed MM. Heat pipe heat exchanger for heat recovery in air conditioning. *Applied Thermal Engineering* 2007; 27: 795-801.  
<http://dx.doi.org/10.1016/j.applthermaleng.2006.10.020>
- [15] Liu G, *et al.* The application of heat pipe heat exchanger in exhaust gas heat recovery and its thermodynamic analysis, 5th International heat pipe symposium, Melbourne, Australia 1996.

Received on 06-07-2015

Accepted on 16-07-2015

Published on 23-09-2015

[DOI: http://dx.doi.org/10.6000/1929-6002.2015.04.03.1](http://dx.doi.org/10.6000/1929-6002.2015.04.03.1)